NIH Public Access
Author Manuscript
Biomaterials. Author manuscript; available in PMC 2015 February 01.

Published in final edited form as:
Biomaterials. 2014 February ; 35(5): 1439–1449. doi:10.1016/j.biomaterials.2013.10.079.

Enhanced GLT-1 mediated glutamate uptake and migration of primary astrocytes directed by fibronectin-coated electrospun poly-L-lactic acid fibers

Jonathan M. Zuidema[1,2], **María C. Hyzinski-García**[3], **Kristien Van Vlasselaer**[1,4], **Nicholas Zaccor**[1,2], **George E. Plopper**[1,4], **Alexander A. Mongin**[3], and **Ryan J. Gilbert**[1,2]

[1]Center for Biotechnology and Interdisciplinary Studies, Rensselaer Polytechnic Institute, Troy, NY 12180, USA

[2]Department of Biomedical Engineering, Rensselaer Polytechnic Institute, Troy, NY 12180, USA

[3]Center for Neuropharmacology and Neuroscience, Albany Medical College, Albany, NY 12208, USA

[4]Department of Biology, Rensselaer Polytechnic Institute, Troy, NY 12180, USA

Abstract

Bioengineered fiber substrates are increasingly studied as a means to promote regeneration and remodeling in the injured central nervous system (CNS). Previous reports largely focused on the ability of oriented scaffolds to bridge injured regions and direct outgrowth of axonal projections. In the present work, we explored the effects of electrospun microfibers on the migration and physiological properties of brain astroglial cells. Primary rat astrocytes were cultured on either fibronectin-coated poly-L-lactic acid (PLLA) films, fibronectin-coated randomly oriented PLLA electrospun fibers, or fibronectin-coated aligned PLLA electrospun fibers. Aligned PLLA fibers strongly altered astrocytic morphology, orienting cell processes, actin microfilaments, and microtubules along the length of the fibers. On aligned fibers, astrocytes also significantly increased their migration rates in the direction of fiber orientation. We further investigated if fiber topography modifies astrocytic neuroprotective properties, namely glutamate and glutamine transport and metabolism. This was done by quantifying changes in mRNA expression (qRT-PCR) and protein levels (Western blotting) for a battery of relevant biomolecules. Interestingly, we found that cells grown on random and/or aligned fibers increased the expression levels of two glutamate transporters, GLAST and GLT-1, and an important metabolic enzyme, glutamine synthetase, as compared to the fibronectin-coated films. Functional assays revealed increases in glutamate transport rates due to GLT-1 mediated uptake, which was largely determined by the dihydrokainate-sensitive GLT-1. Overall, this study suggests that aligned PLLA fibers can promote directed astrocytic migration, and, of most importance, our *in vitro* results indicate for the

Address correspondence to: Ryan J. Gilbert, Ph.D., Associate Professor, Rensselaer Polytechnic Institute, Biomedical Engineering, 110 8th Street, Troy, NY. 12180-3590, Phone: 518 276 2032, gilber2@rpi.edu.

Publisher's Disclaimer: This is a PDF file of an unedited manuscript that has been accepted for publication. As a service to our customers we are providing this early version of the manuscript. The manuscript will undergo copyediting, typesetting, and review of the resulting proof before it is published in its final citable form. Please note that during the production process errors may be discovered which could affect the content, and all legal disclaimers that apply to the journal pertain.

NIH-PA Author Manuscript
NIH-PA Author Manuscript
NIH-PA Author Manuscript

NIH-PA Author Manuscript

NIH-PA Author Manuscript

NIH-PA Author Manuscript

first time that electrospun PLLA fibers can positively modify neuroprotective properties of glial cells by increasing rates of glutamate uptake.

Keywords

Poly-L-lactic acid; Aligned microfibers; Astrocytes; Migration; Glutamate transport; Glutamate metabolism

1. Introduction

Traumatic brain and spinal cord injuries affect approximately 1.7 million people every year in the United States alone [1]. Damage to the central nervous system (CNS) is highly debilitating due to the loss of neurons. Neurons that survive both initial and secondary injury are inhibited by a glial scar that limits regeneration of white matter axons. The small percentage of axons that are able to navigate through the glial scar are not directed due to a lack of guidance cues in the lesion site [2]. One approach to encourage directed axonal regeneration is to use biomaterial guidance scaffolds. Of these, aligned fibers with diameters in the nanometer to micrometer range provide topographic cues that both direct and increase the rate of axonal extension [3–5].

Several different biomaterial fiber approaches have been tested within experimental models of traumatic brain injury (TBI) and spinal cord injury (SCI) with encouraging results. Within TBI models, self-assembling peptide nanofiber scaffolds improve axon regeneration, decrease lesion volumes, and improve functional outcomes [6–7]. Additionally, polycaprolactone (PCL) nanofibers injected into the caudate putamen in rats promote neurite infiltration into the injury cavity 60 days following implantation [8]. Within SCI models, self-assembling IKVAV peptide amphiphile nanofibers promote functional recovery and axon elongation following SCI [9]. Furthermore, fibrous fibronectin channels [10], aligned channels filled with self-assembling peptide nanofibers [11], collagen nanofibers [12], and aligned poly-L-lactic acid (PLLA) microfibers [13] stimulate axonal migration into the biomaterial scaffold.

Further progress in development of biomaterials and their successful introduction into clinical practice may be accelerated through a more comprehensive understanding of their impact on the physiology of glial cells, particularly astrocytes. Astrocytes are the most numerous cells in the CNS, and they play a variety of roles in both healthy and pathological neural tissue. Astrocytes sustain and modulate neuronal activity and viability through the removal of the byproducts of neuronal signaling from the extracellular space, such as K^+ ions and neurotransmitter molecules, and via releasing a plethora of neurotrophins and other biologically active molecules that are collectively termed gliotransmitters [14]. Furthermore, these cells maintain the integrity of the blood-brain barrier and play a pivotal role in coupling neuronal activity to the local rates of blood flow and nutrient metabolism [14–16]. In response to CNS injury, astrocytes undergo the process of reactive gliosis [17–18]. Reactive gliosis is manifested by dramatic phenotypical changes in astrocytes involving cell hypertrophy and upregulation of the intermediate filament proteins, glial fibrillary acidic protein (GFAP) and vimentin. Reactive gliosis also prompts changes in astrocyte cell

NIH-PA Author Manuscript

NIH-PA Author Manuscript

NIH-PA Author Manuscript

physiology and complex reprogramming of gene expression. Reactive gliosis is thought to be of benefit in limiting secondary injury by restricting the spread of toxic and pro-inflammatory substances from the area of damage into healthy CNS parenchyma, limiting the migration of immune cells and removing excitotoxic amino acids. However, reactive changes in astrocytes can be harmful and contribute to tissue injury via uncontrolled secretion of pro-inflammatory cytokines and overproduction of reactive oxygen and nitrogen species [18]. Furthermore, astrocytes create a so-called “glial scar” following CNS injury, generating a physical barrier and producing an extracellular matrix (ECM) that is enriched with chondroitin sulfate proteoglycans. Since the glial scar represents both a physical barrier and a chemical barrier, axonal extension and restoration of neuronal communication is severely inhibited [2].

Extensive experimental evidence in CNS injury, cerebral ischemia, and several other neurological disorders suggests that neurodegeneration and loss of neural functions are largely driven by pathological elevations in extracellular levels of two excitatory amino acids: glutamate and aspartate. The excessive activation of glutamate receptors, particularly their Ca^{2+}-permeable NMDA subtype, leads to a dramatic rise in intracellular Ca^{2+} concentration and initiation of numerous pathological cascades linked to neuronal damage and death [19–21]. Under normal physiological conditions, astrocytes remove extracellular glutamate (and aspartate) via the two astrocyte-specific excitatory amino acid transporters, GLT-1 and GLAST [22]. Once accumulated in the astrocytic cytosol, glutamate is converted to glutamine by the ATP-dependent enzyme glutamine synthetase, which in the CNS is expressed in astrocytes only [23]. Astrocyte-derived glutamine is then released via equilibrating glutamine transporters to the extracellular space, taken-up by neurons, reverted back to glutamate via catalytic activity of glutaminases, and re-packaged in synaptic vesicles for continuous synaptic communication. This cyclical process is termed the brain glutamate-glutamine cycle (for a review see ref. [24]). In pathologies, astrocytes become dysfunctional and dramatically reduce their ability to buffer extracellular glutamate levels. The latter dysfunction has multiple causes: reduced activity of glutamate transporters, metabolic depletion that leads to inhibition of glutamine synthetase, and also astrocytic glutamate loss via several permeability pathways that are activated under pathological conditions [25–26]. Several recent studies found that TBI and SCI lead to chronic down regulation of the astrocytic glutamate transporter GLT-1 [27–30]. Since GLT-1 is the dominant transporter regulating extracellular glutamate levels [31], its loss is thought to contribute to the persistence of the excitotoxic environment preventing neuronal survival, re-establishment of neuronal connections, and re-myelination [32].

The importance of astrocytes following CNS injury has increased recent attention to understanding the effects that biomaterials have on astroglial cells. Biomaterials that shift astrocyte physiology to a more neuroprotective phenotype (e.g., greater expression of glutamate transporters) with less reactivity (e.g., lower GFAP expression) may be valuable in promoting repair following CNS injury. To this point, the general assessment of astrocytes cultured on biomaterials suggests that biomaterials presenting micro- and nanometer topographical features do change astrocyte behavior or elongate the astrocytes to subsequently direct axonal outgrowth. In regards to the astrocytic response to electrospun fibers, astrocytes cultured on PCL nanofibrous mats adhere more strongly, decrease

NIH-PA Author Manuscript

NIH-PA Author Manuscript

NIH-PA Author Manuscript

apoptosis, and increase proliferation in comparison to astrocytes cultured on PCL films [33–35]. Furthermore, GFAP expression is reduced in astrocytes cultured on PCL fibers compared to astrocytes cultured on PCL films, suggesting that topography can reduce this specific marker of astrocyte reactivity [35]. Astrocytes also respond to biomaterials presenting micrometer-sized grooves. Mitotic and colleagues presented data where astrocytes cultured on micropatterned poly(methyl methacrylate) (PMMA) grooved surfaces expressed progenitor markers. The astrocytes expressing these progenitor markers helped direct the extension of neurites [36] similar to an earlier study where astrocytes on polystyrene grooves also become elongated along the grooves to help direct neurite outgrowth [37]. These studies demonstrate that biomaterial topography can change astrocyte behavior and shape to direct neurite outgrowth. However, it is not yet known conclusively whether topographical features can influence other astrocytic functions, particularly the ability of astrocytes to regulate glutamate uptake and metabolism.

In this study, we hypothesized that different PLLA microfiber topographies would cause changes in astrocyte physiology including altered astrocyte migration and glutamate-glutamine metabolism. We tested this hypothesis by plating primary rat astrocytes on fibronectin-coated PLLA films, randomly organized PLLA microfibers, and aligned PLLA microfibers. Following four days of growth and migration we quantitatively compared the rates and directionality of cell migration and changes in cell morphology. Furthermore, we used qPCR, Western blotting, and enzymatic assays to explore changes in the expression levels and activity for several amino acid transporters and enzymes that are critical for glutamate-glutamine metabolism in astroglial cells.

2. Materials and methods

2.1. Film casting

PLLA was chosen to fabricate films and fibers due to its biocompatibility, slow degradation, and the effectiveness of PLLA substrates in promoting robust axonal regeneration in animal models of SCI [13]. PLLA polymer films were cast onto glass coverslips to secure the electrospun fibers to the glass, and the method for casting PLLA onto glass was used as previously described [38]. Briefly, PLLA (Natureworks™; grade 6201D, Cargill Dow LLC, Minnetonka, MN) was dissolved in a 1:1 mixture of the organic solvents chloroform and dichloromethane (Sigma-Aldrich, St. Louis, MO) to make a 4% w/w PLLA solution. 15×15 mm glass coverslips (Knittel Glass, Brausenweig, Germany) were coated with PLLA solution and the solvents were evaporated to form thin PLLA films.

2.2. Fabrication of PLLA microfibers

Aligned, electrospun fiber scaffolds were fabricated using an apparatus described previously [39]. Fibers were produced by electrospinning an 8% (w/w) polymer solution of PLLA dissolved in a 1:1 mixture of dichloromethane and chloroform. The PLLA solution was loaded into a 5 ml syringe (BD Biosciences, Franklin Lakes, NJ) and delivered at a rate of 2.03 ml hr^{-1} through a 22-gauge needle (BD Biosciences) insulated with polymer tubing. Fibers were collected on 15×15 mm glass coverslips coated with the PLLA thin film. The PLLA coated coverslips were secured to a grounded, custom-made aluminum collector disc

NIH-PA Author Manuscript

NIH-PA Author Manuscript

NIH-PA Author Manuscript

(15 cm diameter) with double-sided tape (3M, St. Paul, MN). The distance between the needle tip and the collector disc was set at 6 cm. A high voltage power supply (Gamma High Voltage Research, Ormond, FL) connected to the needle was set at 10 kV, and the rotation speed of the collector wheel was set to 1000 rpm. Fiber samples were collected onto the spinning disc over a period of 20 minutes.

To fabricate randomly oriented fibers, the rotating collector was removed, and a flat conductive aluminum collector was placed below the syringe pump. One 15×15 mm glass coverslip coated with a PLLA film was placed on the flat collector, and randomly oriented fibers were collected over a period of three minutes.

When creating fluorescent aligned or randomly oriented fibers, 10 μg of Rhodamine-B (Sigma-Aldrich) was added to the PLLA solution prior to electrospinning, and the fibers were protected from light exposure until the time of cell seeding.

2.3. Imaging of aligned and randomly oriented fibers

Scanning electron microscopy (SEM) micrographs were captured using a Carl Zeiss Supra55 setup with Direct Write Attachment. The fiber samples were attached to glass slides using conductive copper tape (3M), and the edges of the fibers were secured to the copper tape using Pelco® Colloidal Silver Liquid (Ted Pella Inc., Redding, CA). A Denton Desk IV Sputterer (Denton Vacuum, Moorestown, NJ) coated all the fiber samples with a 5 nm conductive coating of platinum prior to SEM analysis. The operating conditions of the SEM were a 5.00 mm working distance, 20 μm aperture diameter, and an accelerating voltage of 3 kV. Images were captured using a 3:1 mixing ratio of an in-lens secondary electron detector and a Robinson backscattered electron detector. Line integration scanning (n=50 per line) at a reduced scanning rate was used to enhance image resolution.

2.4. Characterization of fiber alignment and diameter

Fiber alignment was characterized using methods described previously [39]. Briefly, a 0° reference line was established using image analysis software. The angle between each analyzed fiber and the reference line was measured. The angle measurements were normalized to the mean angle for each image. The normalized angles were placed into data bins of 2°. The angular difference ranged from 90° to −90° with 0° being the normalized reference line. Scaffolds were considered highly aligned if 95% of the fibers were ± 10° from one another. The absolute value of the angle of deviation was used to plot the data.

The diameter of each fiber was measured perpendicular to the orientation of the fiber. One fiber sample per batch from three independently fabricated batches (fifteen samples per batch) were selected for alignment and diameter analysis. Three SEM images were captured at random locations for each fiber sample. Twenty fibers per image were randomly selected for alignment analysis for a total of 180 fibers. Twenty fibers per image were randomly selected for diameter analysis for a total of 180 fibers. All image analyses were performed using NIH Image J software (NIH, Bethesda, MD).

NIH-PA Author Manuscript

NIH-PA Author Manuscript

NIH-PA Author Manuscript

2.5. Preparation of primary cultures of rat astrocytes

Primary astrocyte cultures were prepared from the cerebral cortex of newborn Sprague-Dawley rats as previously described [40]. All animal procedures in this study strictly adhered to the NIH Guidelines for the Care and Use of Laboratory Animals and were approved by the Institutional Animal Care and Use Committees of Albany Medical College and Rensselaer Polytechnic Institute. Briefly, postnatal day 1 rat pups were euthanized by rapid decapitation. The cerebral cortices were dissected from the meninges, hippocampi, and basal ganglia under sterile conditions. The cortical tissue from four animals was minced in OptiMEM (Invitrogen, Grand Island, NY) and transferred into a solution containing a 1:1 mix of recombinant protease TrypLE and OptiMEM (both Invitrogen). Cells were extracted using three 10-minute incubations with TrypLE/OptiMEM additionally supplemented with 1 mg/ml DNase I (Sigma-Aldrich, St. Louis, MO). The second and third extractions were combined with Dulbecco's Minimal Essential Medium (DMEM, Invitrogen) containing 10% Heat Inactivated Horse Serum (HIHS, Invitrogen) and 50 U/mL penicillin plus 50 μg/mL streptomycin (P/S, Invitrogen). Cells were pelleted using centrifugation (0.5 RCF for 5 min) and resuspended in DMEM/HIHS/P/S. Dissociated cells were plated on poly-D-lysine (Sigma-Aldrich) coated T75 culture flasks at a density of 200,000 cells/flask. Astrocytes used in the study were cultured for 2–4 weeks until reaching a confluent state and used for subsequent procedures as described below. The purity of astrocytic cultures (>95% pure) was periodically verified using staining with an antibody for the astrocytic marker glial fibrillary acidic protein (GFAP) (Dako, Glostrup, Denmark).

2.6. Plating astrocytes on PLLA films and electrospun fiber scaffolds

PLLA films, randomly oriented fibers, and aligned fibers were sterilized for 12 hours using ethylene oxide (AN74i, Andersen Sterilizers, Haw River, NC). Prepared films and fiber scaffolds were then plasma treated for 90 seconds using a Plasma Cleaner (Harrick Plasma, Ithaca, NY). Components within the extracellular matrix (ECM) are known to regulate astrocyte behavior [41–42]. In order to determine the best ECM coating for the PLLA fibers that promoted robust astrocyte adhesion, astrocytes were seeded on aligned PLLA fibers that were coated overnight with fibronectin (Sigma-Aldrich), laminin (Invitrogen), or collagen I (Invitrogen) at a concentration of 10 μg/mL. Cell number was calculated using ImageJ to quantify the number of cells stained with DAPI. Three images from three independent cultures (n=9) were evaluated to determine the number of cells adhered to collagen 1, laminin, and fibronectin coated aligned PLLA fibers. Fibronectin coating provided superior astrocyte attachment, as compared to all other ECM molecules (Supplemental Fig. S1). Therefore, fibronectin coating was used in all the subsequent experiments. Astrocytes were seeded at a concentration of 1,000 cells/mm^2, and were cultured for four days before fixation for immunocytochemical analyses, protein collection, polymerase chain reaction (PCR), or glutamate assays. To acquire images of individual cells (such as for visualizing fluorescent fibers and GFAP staining), astrocytes were plated at a much lower density of 100 cells/mm^2.

NIH-PA Author Manuscript

NIH-PA Author Manuscript

NIH-PA Author Manuscript

2.7. Immunocytochemistry

After four days in culture, astrocytes were fixed in 4% paraformaldehyde. Cells were blocked and permeabilized with 0.4% Triton-X (Sigma-Aldrich) and 5% bovine serum albumin (BSA, Sigma-Aldrich) in phosphate buffered saline (PBS, Life Technologies, Grand Island, NY). Primary antibodies were applied to the scaffolds using the following concentrations: rabbit anti-GFAP (1:700, Z0334, Dako), rabbit anti-GLT-1 (1:40, Abcam, Cambridge, UK, ab41621), and mouse anti-α-tubulin (1:900, Sigma-Aldrich, T6199). Phalloidin (Life Technologies) was used at a dilution of 1:400, and DAPI (Sigma-Aldrich) was used at a concentration of 1 μg/mL. The secondary antibodies used were Alexa-Fluor anti-mouse 598 (1:1000, Life Technologies) and Alexa-Fluor anti-rabbit 488 (1:1000, Life Technologies). All images were taken on an inverted Olympus IX-81 microscope (Olympus, Tokyo, Japan). Fluorescent images were taken at 40× magnification unless otherwise specified, and images were assembled using Adobe Photoshop CS5 (Adobe, San Jose, CA).

2.8. Cytoskeletal alignment

Alignment of cytoskeletal fibers, either actin filaments or microtubules, was determined using the OrientationJ plugin for ImageJ as described previously [43]. Three 40× images captured from three independent cultures (n=9) for a total of nine images were analyzed for each scaffold type. A circle with a radius of 2 μm was drawn, and 10 areas within cells in each image were analyzed using the circle. The median angle of the cytoskeletal fibers in each image was determined. The angles determined in each image were compared to the image's median angle, and these angles were averaged for each of the three scaffold conditions.

2.9. Evaluation of nuclear morphology and alignment

Nuclei alignment and morphology were analyzed using ImageJ. Three images from three independent cultures (n=9) were analyzed for the three scaffold conditions. Lines were drawn on the image to determine the length of the long axis and short axis of the nuclei. The nuclear aspect ratio (NAR) was determined by dividing the long axis by the short axis (NAR = Long axis/Short axis). The angle of the long axis was used to determine nuclei alignment. The median angle of all nuclei in an image was determined for each image analyzed, and the difference between the median angle and the angle of each nuclei was averaged to determine nuclei alignment

2.10. Migration assay

PLLA film, randomly oriented fiber, and aligned fiber samples were coated using a concentration of 20 μg/mL fibronectin overnight at 37°C. Sterile glass cloning cylinders were placed on each scaffold and 50,000 primary astrocytes were seeded into each glass cylinder for 12 hours. Once the cylinders were removed, samples were either fixed immediately for the 0 hour time point (n=3) or allowed to incubate for 96 hours (n=3). Samples were then stained with Phalloidin and DAPI, 10× images were taken using an Olympus IX81 fluorescence microscope, and the migration was quantified as described below. Astrocytes formed nearly circular, uniform monolayers after the initial incubation period. The length of the longest axis of this area at t = 0 for the three PLLA scaffolds (film,

NIH-PA Author Manuscript

NIH-PA Author Manuscript

NIH-PA Author Manuscript

randomly oriented, and aligned) using the Ferets Diameter feature in ImageJ was measured. These measurements defined a circle that served as the migration distance equal to 0. Over time, cells began to migrate, distorting the circular area covered by cells. The distance of migration was defined as the length of the longest axis of cell area and the distance 90° from the long axis (long and short axes, respectively).

2.11. RNA isolation and quantitative RT-PCR

Messenger RNA was isolated from cultured astrocytes using RNAqueous®-4PCR kit (Ambion, Austin, TX) according to the manufacturer's instructions. The concentration of mRNA in each sample was determined using a ND-100 NanoDrop® spectrophotometer (NanoDrop Technologies, Wilmington, DE). cDNA was prepared from mRNA using the iScript Reverse Transcriptase cDNA synthesis kit according to the manufacturer's instructions (Bio-Rad, Hercules, CA). The relative expression of genes of interest was determined by quantitative PCR using iTaq SYBRGreen Supermix (Bio-Rad) and a CFX96/C1000 thermocycler (Bio-Rad). We utilized the following validated QuantiTect® primers (Qiagen, Valencia, CA): glutaminase 1 (catalog # Rn_Gls_1_SG), glutaminase 2 (Rn_Gls2_1_SG), glutamine synthetase (Rn_Glul_2_SG), glutamate dehydrogenase 1 (Rn_Glud1_1_SG), GLAST (Rn-Slc1a3_1_SG), GLT-1 (Rn_Slc1a2_1_SG), system N amino acid transporter 1 (Rn_Slc38a3_1_SG), and system N amino acid transporter 2 (Rn_Slc38a5_1_SG). Expression levels for each gene of interest were normalized to the intra-sample levels of two housekeeping genes, RPL13A (Rn-Rpl13_1_SG) and GAPDH (Rn_Gapd_1_SG), and normalized expression levels of mRNA isolated from six independent cultures (n=6) were averaged and compared.

2.12. Determination of astrocyte protein expression

Protein levels in cultured astrocytes were determined by a quantitative Western blot approach. Cells grown in 100 mm dishes on ten 15×15 mm coverslips of each scaffold type were lysed in a solution containing 2% sodium dodecyl sulfate (SDS) plus 8 mM EDTA. The total protein concentration in the lysates was determined using a colorimetric bicinchoninic acid (BCA) assay kit (ThermoFisher Scientific/Pierce, Rockford, IL). The lysates were subsequently diluted with a reducing Laemmli buffer and stored at −20°C before being utilized for the assay. 15 μg of total protein were loaded into each lane of a 10% polyacrylamide gel and electrically separated. Separated proteins were transferred onto an Immuno-Blot™ polyvinylidene difluoride (PVDF) membrane (Bio-Rad). The membranes were blocked with 5% non-fat milk in Tris-buffered saline (TBS) containing 0.05% Tween 20 (TBST). The membranes were then incubated overnight at 4°C with polyclonal anti-GLT-1 antibody (1:200, Abcam, ab41621), polyclonal anti-GLAST antibody (1:4,000, Abcam, ab416), or polyclonal anti-glutamine synthetase antibody (1:20,000, Sigma-Aldrich, G2781). To visualize protein signal, membranes were further incubated with horseradish peroxidase (HRP)-conjugated secondary antibodies (1:10,000, GE Healthcare/Amersham Biosciences, Piscataway, NJ) for 1 hr at room temperature. The HRP signal was detected using a chemiluminescence ECLplus substrate (GE Healthcare/Amersham Biosciences) in a LAS-400 image analyzer (FujiFilm Medical Systems, Stamford, CT). PVDF membranes were additionally stripped and re-probed with a monoclonal anti-actin antibody (1:1,000, Abcam, ab3280) to assure equal levels of protein loading. Intensities of

NIH-PA Author Manuscript

NIH-PA Author Manuscript

NIH-PA Author Manuscript

immunofluorescent bands on Western blots using protein isolated from four independent cultures (n=4) were quantified using ImageJ software and additionally normalized to the actin loading levels on the same PVDF membranes.

2.13. Glutamate transport assay

To determine glutamate uptake, astrocytes grown on five 15×15 mm coverslips of each scaffold type were transferred into 60-mm dishes, with five coverslips per dish. Cells were washed three times from serum-containing media with HEPES buffered basal medium of the following composition: 135 mM NaCl, 3.8 mM KCl, 1.2 mM $MgSO_4$, 1.3 mM $CaCl_2$, 1.2 mM KH2PO4, 10 mM D-glucose, and 10 mM HEPES (pH 7.4 adjusted with NaOH). To perform the uptake assay astrocytes were incubated for 30 min at 37°C in the basal medium containing 0.5 μCi/mL of L-[^{3}H]glutamate (PerkinElmer/New England Nuclear, Waltham, MA) plus 2 μM of unlabeled L-glutamate. Glutamate uptake was terminated by three washes with ice-cold basal medium and cells were lysed in 1 mL of 2% SDS plus 8mM EDTA. 100-μL aliquots of the lysates were taken to determine protein content using the BCA protein assay kit (see above). The remaining lysates were collected into scintillation vials and 4 mL of Ecoscint A scintillation fluid (National Diagnostics, Atlanta GA) was added to each sample. [^{3}H] content was analyzed with a TriCarb 2900TR scintillation counter (PerkinElmer). Glutamate uptake rates (10–26 independent assays performed in 3–9 different cultures) were calculated based on L-[^{3}H]glutamate specific activity and normalized to protein content in each well. In order to determine the relative contribution of the glutamate transporter GLT-1, we utilized dihydrokainate (DHK), which is a GLT-1 inhibitor that discriminates GLT-1 from other glutamate transporters [44]. When DHK was used, 1mM DHK was incorporated into the astrocyte cultures and incubated with the L-[^{3}H]glutamate.

2.14. Determination of glutamine synthetase activity

Glutamine synthetase activity was determined as described elsewhere [40]. Briefly, cells grown on 15×15 mm coverslips covered with various substrates were washed with basal HEPES-buffered medium (for composition see above). They were then transferred into 60-mm dishes, five coverslips per dish, and pre-incubated in the basal medium additionally containing 1 mM of the irreversible glutaminase inhibitor 6-diazo-5-oxo-L-norleucine (DON, Sigma-Aldrich) for 40 min. This treatment prevents hydrolysis of newly formed glutamine by intracellular glutaminases [40]. Cells were then washed two times with basal medium, and incubated with glutamine synthetase substrates 2 μCi/mL L-[^{3}H]glutamate, 2 μM unlabeled L-glutamate, and 100 μM $(NH_4)_2SO_4$ in the basal medium for 30 minutes at 37°C. Extracellular isotope was removed, cells were washed with ice-cold basal medium three times, and subsequently lysed in hypoosmotic solution containing 1 mM EDTA plus 5 mM HEPES (pH 7.4). The lysates were transferred onto AG1-X8 Polyprep anion exchange columns (Bio-Rad). Loaded intracellular L-[^{3}H]glutamate was separated from newly synthesized L-[^{3}H]glutamine by sequential elution with distilled H_2O and 0.1 M HCl to collect glutamine and glutamate, respectively. Ecoscint A scintillation fluid was added to vials containing eluent fractions, and the [^{3}H]-labeled amino acid content was quantified in a Tri-Carb 2900TR liquid scintillation analyzer. Glutamine synthetase activity from six

NIH-PA Author Manuscript

NIH-PA Author Manuscript

NIH-PA Author Manuscript

independent cultures (n=6) was determined as the enzymatic production of L-[^{3}H]glutamine expressed as the percentage fraction of the total amount of intracellular [^{3}H].

2.15. Statistical Analysis

All data are presented as mean values ± standard error of the mean (SE). Statistical comparisons of fiber diameter, cytoskeletal alignment, migration analysis, astrocyte adhesion, nuclei morphology, glutamate uptake, and GS activity were done using ANOVA followed by the Tukey-Kramer post hoc test for multiple comparisons. Differences with $p<0.05$ were considered significant. For data sets that were normalized to within-experiment controls (qRT-PCR and Western blots) a t-test with the Bonferroni correction for multiple comparisons was used to determine statistical significance. Origin 8.0 (OriginLabs, Northampton, MA) or Prism 5.01 (GraphPad Software, San Diego, CA) were used for all statistical analyses.

3. Results

3.1. Fiber Morphology

We started our work with characterization of the PLLA scaffolds. PLLA films (Fig. 1A), randomly oriented fibers (Fig. 1B), and aligned fibers (Fig. 1C) were imaged using a scanning electron microscope to determine surface topography, fiber diameter, and fiber alignment. PLLA thin films, which were used as controls to represent non-topographical substrates, had very smooth surfaces with no topographical features (Fig. 1A). Quantification of fiber alignment showed that randomly oriented fibers had no preferential orientation and had a distribution of angle deviation over the entire range of angles (Fig. 1E). Aligned fibers deviated no more than 10° from the median angle of alignment (Fig. 1F), showing the collection wheel did create highly aligned fiber samples. Randomly oriented PLLA fibers had an average diameter of 2.38 ±0.46 μm, while the aligned PLLA fibers had an average diameter of 2.49 ±0.32 μm (Fig. 1D). There was no statistically significant difference in the diameters between the two types of fiber preparations. The latter fact is important since any changes seen in astrocyte behavior cannot be explained by differences in fiber diameter between randomly oriented and aligned preparations.

3.2. Adhesion and morphology of primary astrocytes on PLLA scaffolds

After investigating the effect of ECM coating on astrocyte adhesion to aligned fiber substrates (shown in Supplemental Fig. 1), we found that astrocytes adhered strongly, and the adhesion was uniform on aligned fiber surfaces. Fibronectin coating was superior in sustaining astrocyte survival and proliferation (Supplemental Fig. 1) and was used in all subsequent experiments. We next examined if substrate topology affects astrocytic adhesion and morphology. With this purpose, we compared cells plated on fibronectin-coated randomly oriented and aligned PLLA fibers to cells seeded on PLLA films. Astrocytes were plated onto all three substrates at low and high seeding densities. Low magnification (4×) images of astrocytes on PLLA films (Fig. 2A), randomly oriented fibers (Fig. 2B), and aligned fibers (Fig. 2C) were taken to show that astrocytes do indeed form a confluent layer on all three PLLA substrates when coated with fibronectin. These 4× images were also used to observe the overall orientation of astrocytes on the three scaffolds. Astrocytes cultured on

NIH-PA Author Manuscript

NIH-PA Author Manuscript

NIH-PA Author Manuscript

PLLA films and randomly oriented fibers show no preferential orientation of process extension, but astrocytes orient parallel to the fibers when cultured on the aligned fiber scaffolds. High magnification (40×) images of low-density astrocyte cultures were used to show the morphology of individual cells. Astrocytes cultured on PLLA films (Fig. 2D) show no significant process extension, but instead display a spread morphology with no preferential direction of process extension. Astrocytes cultured on randomly oriented fibers (Fig. 2E) have several processes that extend non-preferentially in all directions. The processes extend as long as 200 μm, but most extend approximately 50 μm. Also, the processes seem to extend without being guided by any specific fiber. Astrocytes cultured on aligned fibers, (Fig. 2F) extend several processes in the direction of fiber orientation. The processes of these astrocytes extend longer than the processes on randomly oriented fibers, extending up to 400 μm, with most processes being around 200 μm in length. Contrary to astrocytes cultured on randomly oriented fibers, the processes of these astrocytes appear to be directed by single fibers. These results show that fibronectin coating through adsorption onto PLLA surfaces supports uniform, confluent adhesion on all PLLA surfaces. Additionally, astrocytes on fiber surfaces do respond to topography by sending out processes that are either directed along the fibers (on aligned fibers substrates) or are undirected without seemingly following fiber topography (on randomly oriented substrates).

3.3. Cytoskeletal organization of F-actin and tubulin within primary astrocytes cultured on PLLA scaffolds

Astrocytes respond to topographical features by extending and elongating in the presence of a topographical cue. Of question is whether the extension and elongation is supported by actin and/or tubulin cytoskeletal elements. To answer this question, astrocytes on aligned PLLA fibers, randomly organized fibers, and control films were stained against actin and tubulin cytoskeletal elements. F-actin of astrocytes cultured on PLLA films (Fig. 3A, D °=45.24 ±11.13) and randomly oriented fibers (Fig. 3B,D °=37.03 ±10.52) showed no preferential orientation. Similarly to the overall morphology of astrocyes, F-actin of astrocytes cultured on the aligned fibers (Fig. 3C) showed a preferential orientation in the direction of the fibers (Fig. 3D °=4.84 ±1.55). Tubulin staining revealed a similar trend. There was no preferential alignment of microtubules in astrocytes cultured on PLLA films (Fig. 3E,H °=43.96 ±10.82) or randomly oriented fibers (Fig. 3F,H °=32.61 ±10.55), but microtubules of astrocytes cultured on aligned fibers were oriented in the direction of the aligned fibers (Fig. 3G,H °=4.79 ±1.42). These results show that fibers have the ability to alter the orientation of the cytoskeletal proteins that support astrocyte cell structure.

3.4. Astrocyte migration on PLLA scaffolds

Previously, our group studied astrocyte migration on poly-D-lysine coated PLLA films, randomly oriented fibers, and aligned fibers using a gap model where astrocytes on either side of the gap migrated into the gap over time [13]. In the present study, a different migration assay was used. Here, we assessed astrocyte migration away from a grouping of cells isolated to a specific part of each scaffold using a cloning cylinder to keep the cells in a specific location before beginning migration. The present astrocyte migration method was used to assess cell migration that is not influenced by factors released from a disconnected cell group. The importance of conducting these experiments is in evaluating the potential of

NIH-PA Author Manuscript

NIH-PA Author Manuscript

NIH-PA Author Manuscript

a biomaterial to promote astrocyte migration, as astrocyte migration into and through a lesion is necessary for healing of the injured CNS. Additionally, it was unknown if fibronectin presence would change the migration capacity of astrocytes in the presence or absence of topography. Four days after the cloning cylinder was removed, the longest axis of astrocyte migration and the extension perpendicular to the longest axis of astrocyte migration were determined. Representative images from the longest axis of migration or perpendicular to the longest axis of migration are shown so that differences in directional migration can be viewed. Astrocytes cultured on PLLA films (Fig. 4A, B) or randomly oriented fibers (Fig. 4C, D) showed little migration preference in any particular direction and migrated between 527–551 ±51 μm and 476–561 ±6.5 μm, respectively (Fig. 4G). Astrocytes cultured on aligned PLLA fibers showed a different migration behavior. On aligned fiber scaffolds, there was less migration (217 ±98 μm) in the direction perpendicular to the long axis of migration (Fig. 4E) and significantly more migration (766 ±75 μm) in the direction of the longest axis of growth (Fig. 4F). Also, there was significantly more migration in the direction of the longest axis of astrocytes cultured on aligned fibers compared to astrocytes cultured on films and randomly oriented fibers (Fig. 4G). The longest axis of migration was parallel to fiber alignment, showing the ability of aligned fibers to direct and increase the migration rate of astrocytes. Astrocytes were able to elongate up to 400 μm over four days on aligned fibers (Fig. 2F), so some of the increased distance traversed by astrocytes on aligned fibers may be due to process elongation and not just simply cellular migration. Regardless, these results confirm that the presence of fibronectin on electrospun fibers does promote astrocyte migration and elongation dependant on the alignment of the fibers.

3.5. Effects of substrate topology on mRNA and protein expression of the molecules and enzymes required for glutamate and glutamine transport and metabolism

In order to explore if substrate topology affects the physiology of cultured astrocytes, we performed quantitative RT-PCR and Western blot analyses for a battery of gene products involved in glutamine and glutamate transport and metabolism. The genes of interest included the astrocyte specific glutamate transporters, GLT-1 and GLAST, the glutamine transporters, SNAT3 (SN1) and SNAT5 (SN2), the glutamate-metabolizing enzymes, glutamine synthetase (GS) and glutamate dehydrogenase (GDH), and the glutamine hydrolyzing enzymes, glutaminases 1 and 2 (GLN1 and GLN2). As seen in Fig. 5A–B, mRNA levels for three of the above mentioned enzymes, GLT-1, GLAST, and GS showed a trend for approximately two-fold upregulation in cells cultured on PLLA fibers, independent of fiber orientation ($p<0.1$). However, these effects did not reach the level of statistical significance due to variability between cell cultures. One of GLN's isoforms, the phosphate-activated GLN2, was consistently and significantly down regulated by 35–40% in cells grown on both randomly oriented and aligned fibers. We further investigated the effects of fiber scaffolds on protein expression levels for the gene products that showed a trend for upregulation. Data presented in Fig. 5C–F indicate that GLT-1, GLAST, and GS were upregulated on a protein level on either random or aligned fibers, or both. Taken together, the correlation of qRT-PCR and Western blot data strongly suggests that substrate topology has an impact on the protein expression of astroglial cells.

NIH-PA Author Manuscript

NIH-PA Author Manuscript

NIH-PA Author Manuscript

3.6. Effects of scaffold topology on glutamate uptake and GS activity

To determine if the PLLA fiber-dependent changes in protein levels are functionally significant, we first examined glutamate transport rates in cells cultured on different substrate topologies. As shown in Fig. 6A, in the cells grown on either randomly oriented or aligned fibers, glutamate uptake was significantly increased by 35–50% as compared to PLLA films. In order to determine which subtype of glutamate transporter (GLAST or GLT-1) contributes to the observed increase in uptake values, we utilized the GLT-1 selective inhibitor, dihydrokainate (DHK) [44]. DHK significantly reduced glutamate accumulation only in cells plated on randomly oriented or aligned fibers, with no effect observed in cells cultured on films fabricated from the same PLLA material. These results parallel the mRNA and protein expression data and implicate for the first time functional GLT-1 upregulation induced by fibronectin-coated PLLA microfibers.

With the same purpose, we measured GS activity in astrocytes grown on the same three substrate topologies. In GS activity assays, we found high GS activity rates in all experimental groups. Within 30 minutes, ∼60% of L-[^{3}H]glutamate, which was accumulated inside astrocytes, was converted to L-[^{3}H]glutamine. Our previous study established that such conversion is completely mediated by astrocytic GS [40]. However, we observed no significant changes in GS activity between experimental groups (Fig. 6B), even though GS protein levels were significantly upregulated by >50% in cells grown on aligned fibers (see Fig. 5F). Potential reasons for discrepancies between protein expression and activity levels are addressed in the Discussion.

3.7. GLT-1 Immunocytochemistry

To further validate the changes in the expression and function of glutamate transporters, we performed additional immunocytochemical analysis for GLT-1, which is known to regulate glutamate levels in vivo [45]. Astrocytes cultured on PLLA films (Fig. 7A), randomly oriented fibers (Fig. 7B), and aligned fibers (Fig. 7C) were stained against GLT-1 and F-Actin. As seen in this figure, astrocytes cultured on PLLA fibers appear to have more intense staining of GLT-1 than astrocytes on PLLA fibers, which is analogous to the upregulation of GLT-1 seen through Western blots and functional assays.

4. Discussion

The major findings of this study are: (1) we identified the most suitable fiber coating, fibronectin, that sustains astrocytic interactions with microfibers, (2) we demonstrated that bioengineered scaffolds consisting of the aligned PLLA fibers can promote directed astrocytic migration along the fiber material, and (3) we further discovered that the PLLA scaffold topology has unexpected and potentially beneficial effects on astroglial cells that involve upregulation of “neuroprotective” proteins involved in removal of extracellular glutamate (GLAST and GLT-1) and glutamate metabolism (glutamine synthetase or GS). This is an important extension of our previous *in vitro* and *in vivo* work, which established that aligned PLLA microfibers promote guided axonal growth and allow for bridging of transected spinal cord tissue [13]. Although the current results will have to be further validated *in vivo*, our work represents an important step towards mechanistic understanding

NIH-PA Author Manuscript

NIH-PA Author Manuscript

NIH-PA Author Manuscript

of interactions between biomaterials and astrocytes and the development of therapeutic approaches for traumatic brain and spinal cord injuries.

Design of biomaterials for repair of the injured CNS requires consideration of several factors that include biomaterial surface topography and the incorporation of proteins and/or cytokines that promote axonal regeneration and the migration of beneficial cells, such as astrocytes, into the lesion site. For CNS applications, electrospun fibers provide surface topography that can direct axonal regeneration within the injured spinal cord when the fibers are highly aligned [13]. While topography alone is able to direct regeneration, several recent studies attempt to improve the rate of axonal regeneration through the inclusion of an extracellular matrix compound(s). Laminin that is adsorbed or covalently coupled to the surface of fibers has been shown to increase the length of extending neurites [46–47]. Also, fibers containing collagen promote better axonal guidance than scaffolds without collagen [48]. However, while collagen and laminin may help promote adhesion and neurite extension respectively, it is largely unknown how specific ECM molecules on the surface of electrospun fibers influence astrocytes. We found that a fibronectin coating on PLLA aligned fibers promote stronger adhesions by astrocytes when compared to aligned PLLA fiber surfaces that were coated with laminin or collagen (Supplemental Fig. 1). Furthermore, fibronectin coating of PLLA surfaces with no topography or randomly organized fibers also supported uniform adhesion of astrocytes (Fig. 2). Therefore, while laminin incorporation may be necessary to promote faster axonal regeneration, incorporation of fibronectin into an electrospun fiber strategy may better support astrocyte migration and adhesion, leading to better regeneration outcomes overall.

Both aligned and randomly organized electrospun fibers induced astrocytes to form long cellular processes (Fig. 2), and on aligned electrospun fibers in particular, both F-actin and tubulin cytoskeletal structures (Fig. 3) and the nuclear alignment (Supplemental Fig. 2) were organized parallel to the aligned fiber orientation. The NAR of astrocytes cultured on aligned fibers was also significantly higher than astrocytes cultured on PLLA films or randomly oriented fibers (Supplemental Fig. 2). Astrocyte migration was most pronounced along the aligned fiber substrate as well (Fig. 4). The link between the above results (aligned cytoskeleton, nuclear alignment and NAR, and enhanced migration along the aligned fibers) suggests that a highly structured cytoskeleton and an aligned and stretched nucleus may increase migration of a cell that is parallel to the alignment of the cytoskeleton. The relationship between the speed of cellular migration and nuclear alignment and NAR was also observed in studies analyzing C2C12 mouse myoblast migration along fibronectin-coated aligned polystyrene nanofibers [49]. It may also be that astrocyte migration on randomly organized fibers is slowed due to the crossing of fibers and lack of consistent cellular guidance that aligned fibers provide. Crossing fibers are known to stop neurite extension [39], suggesting that a physical barrier could also slow astrocyte migration or change cytoskeletal structure and nuclear shape in a manner that diminishes pronounced migration in a particular direction.

Few studies to this point have examined the ability of electrospun fibers to affect astrocytic production of markers indicative of enhanced reactivity (e.g., increased production of GFAP) or greater capability of neuroprotection (e.g., increased production of glutamate

NIH-PA Author Manuscript

NIH-PA Author Manuscript

NIH-PA Author Manuscript

transporters, increased glutamate uptake). In terms of studying changes in astrocyte physiology related to neuroprotection on electrospun fibers, GLT-1 gene expression was only recently analyzed from astrocytes cultured on laminin-coated electrospun fibers created from polyurethane resin [50]. In this latter study, the randomly organized fiber matrix did not significantly affect GLT-1 gene expression.

Unlike the study published by Puschmann and colleagues [50], the present study shows that astrocytes cultured on fibronectin-coated PLLA fibers significantly increased their expression of two glutamate transporters, GLAST and GLT-1, as compared to PLLA film controls (Fig. 5). Additionally, data presented here is the first example of electrospun fiber topography increasing astrocyte glutamate uptake. The glutamate uptake was increased largely due to the increased expression and function of GLT-1 (Fig. 5–7). Although there was a significant increase in GLAST expression in astrocytes cultured on randomly oriented fibers compared to films (Fig. 5), this increase did not lead to a significant change in glutamate uptake when GLT-1 uptake was blocked by DHK under our experimental conditions (Fig. 6).

Also of importance, expression of the glutamate-metabolizing enzyme GS was up-regulated by astrocytes cultured on aligned PLLA fibers (Fig. 5). However, in functional assays we found no functional changes in the GS activity between the three groups (Fig. 6). The astrocytes proportionally converted the same percentage of glutamate to glutamine on all three PLLA substrates. Potential reasons for differences between protein expression and functional assays are: (a) enzyme is produced but is not delivered to the cellular compartment responsible for glutamate-to-glutamine conversion, or (b) the experimental conditions in GS assays make substrate availability, rather that enzymatic levels, rate limiting. We think that the second possibility is more likely because we used very low L-[^{3}H]glutamate levels, as compared to the expected local levels of glutamate in vivo.

Since this is the first study revealing the ability of a biomaterial to influence astrocytic upregulation of glutamate transporters and subsequent improvement of glutamate uptake, the significance of such a finding has great potential to improve regeneration following CNS injury. Following CNS injury, extracellular glutamate levels increase transiently to neurotoxic levels within three hours after initial trauma. There are also subacute (2–3 days) and delayed (7+ days) events leading to increases in extracellular glutamate concentrations; mainly mitochondrial dysfunction of axons and oligodendrocytes that lead to further release of glutamate [51]. Therefore, biomaterials implanted into the site of injury that can enhance astrocytic ability to uptake more glutamate may lead to better regenerative outcomes. Additionally, it is well known that the glutamate transporter, GLT-1, is down regulated following CNS injury [27–30]. GLT-1$^{+/-}$ heterozygous mice that exhibit lower expression of GLT-1 compared to control mice show worse functional outcomes following SCI [30]. Increasing GLT-1 expression with 17β-oestradiol treatment [28] or using an adeno-associated viral vector expressing rat GLT-1 [52] improved functional outcomes following spinal cord injury and ischemic brain injury, respectively. The success of these therapeutic strategies suggests that biomaterials that can induce astrocytes to upregulate production of GLT-1, like the fibronectin-coated PLLA fibers presented here, may help promote astrocytes to construct a post-injury environment that is suitable for extensive axon regeneration.

NIH-PA Author Manuscript

NIH-PA Author Manuscript

NIH-PA Author Manuscript

Constructing electrospun fiber scaffolds with defined physical characteristics may be necessary to shift astrocytes towards a more neuroprotective phenotype. Specific fiber diameters or specific fiber surface treatments may elicit the appropriate presentation of physical factors and ECM ligands to induce astrocyte changes. It is known that electrospun fiber diameter can influence the ability of oligodendrocytes to produce myelin [53]. The results of this study by Lee *et al*. suggest that the length of fiber diameters could also influence astrocytes to increase glutamate transporter production and glutamate uptake. Additionally, the presence of specific extracellular matrix legends on the surface of the fibers may work in concert with the geometrical shape of the fibers to induce changes in astrocyte physiology. Laminin-coated polyurethane fibers did not significantly change GLT-1 expression, but the fibronectin-coated PLLA fibers presented here did. Such questions concerning fiber diameter and potential synergism between diameter and presentation of ECM molecules are currently being examined. The differences between these studies suggests that careful consideration of electrospun fiber physical characteristics and coating procedures should be made prior to experimentation in order to isolate key parameters responsible for inducing changes in astrocyte physiology.

5. Conclusion

Electrospun fiber scaffolds are increasingly utilized to provide topographical cues that aid in directing cellular and axonal migration in animal models of CNS injury. In this study, we found that aligned PLLA electrospun fibers strongly promote directed astrocytic migration when compared to the randomly oriented fibers or PLLA films. Furthermore, coating of the PLLA fibers with fibronectin strongly improved astrocytic adhesion and survival, suggesting that this modification may be helpful in future development of bioscaffolds for in vivo use. Most importantly, the fibronectin-coated PLLA fibers produced unexpected and significant changes in astrocyte physiology as compared to PLLA films. Specifically, we discovered that the fiber topology causes upregulation of expression and function of glutamate transporters, particularly GLT-1, and increases levels of the glutamate-metabolizing enzyme glutamine synthetase. If the same PLLA fiber effects will be preserved in vivo, the bioscaffolds identified by us may create a neuroprotective environment that is more hospitable for subsequent axonal regeneration.

Supplementary Material

Refer to Web version on PubMed Central for supplementary material.

Acknowledgments

This work was supported by NSF CAREER Award 1105125 to RJG and NIH grant R01 NS061953 to AAM.

References

1. Faul M, Xu L, Wald MM, Coronado VG. Traumatic Brain injury in the United States: emergency department visits, hospitalizations, and deaths. Atlanta (Ga): Centers for Disease Control and Prevention. National Center for Injury Prevention and Control. 2010
2. Silver J, Miller JH. Regeneration Beyond The Glial Scar. Nat Rev Neurosci. 2004; 5:146–156. [PubMed: 14735117]

NIH-PA Author Manuscript

NIH-PA Author Manuscript

NIH-PA Author Manuscript

3. Cao H, Liu T, Chew SY. The application of nanofibrous scaffolds in neural tissue engineering. Adv Drug Deliv Rev. 2009; 61:1055–1064. [PubMed: 19643156]
4. Madigan NN, McMahon S, O'Brien T, Yaszemski MJ, Windebank AJ. Current tissue engineering and novel therapeutic approaches to axonal regeneration following spinal cord injury using polymer scaffolds. Respir Physiol Neurobiol. 2009; 169:183–199. [PubMed: 19737633]
5. Gilbert RJ, Rivet CJ, Zuidema JM, Popovich PG. Biomaterial design considerations for repairing the injured spinal cord. Crit Rev Biomed Eng. 2011; 39:125–180. [PubMed: 21488818]
6. Ellis-Behnke RG, Liang Y, You S, Tay DKC, Zhang S, So K, et al. Nano neuro knitting: Peptide nanofiber scaffold for brain repair and axon regeneration with functional return of vision. Proc Natl Acad Sci U S A. 2006; 103:5054–5059. [PubMed: 16549776]
7. Guo J, Leung KK, Su H, Yuan Q, Wang L, Chu TH, et al. Self-assembling peptide nanofiber scaffold promotes the reconstruction of acutely injured brain. Nanomedicine. 2009; 5:345–351. [PubMed: 19268273]
8. Nisbet DR, Rodda AE, Malcolm KH, Forsythe JS, Finkelstein DI. Neurite infiltration and cellular response to electrospun polycaprolactone scaffolds into the brain. Biomaterials. 2009; 30:4573–4580. [PubMed: 19500836]
9. Tysseling-Mattiace VM, Sahni V, Niece KL, Birch D, Czeisler C, Fehlings MG, et al. Self-assembling nanofibers inhibit glial scar formation and promote axon elongation after spinal cord injury. J Neurosci. 2008; 28:3814–3823. [PubMed: 18385339]
10. Phillips JB, King VR, Ward Z, Porter RA, Priestley JV, Brown RA. Fluid shear in viscous fibronectin gels allows aggregation of fibrous materials for CNS tissue engineering. Biomaterials. 2004; 25:2769–2779. [PubMed: 14962555]
11. Gelain F, Panseri S, Antonini S, Cunha C, Donega M, Lowery J, et al. Transplantation of Nanostructured composite scaffolds results in the regeneration of chronically injured spinal cords. ACS Nano. 2011; 5:227–236. [PubMed: 21189038]
12. Liu T, Houle JD, Xu J, Chan BP, Chew SY. Nanofibrous collagen nerve conduits for spinal cord repair. Tissue Eng Part A. 2012; 18:1057–1066. [PubMed: 22220714]
13. Hurtado A, Cregg JM, Wang HB, Wendell DF, Oudega M, Gilbert RJ, et al. Robust CNS regeneration after complete spinal cord transection using aligned poly-L-lactic acid microfibers. Biomaterials. 2011; 32:6068–6079. [PubMed: 21636129]
14. Haydon PG, Carmignoto G. Astrocyte control of synaptic transmission and neurovascular coupling. Physiol Rev. 2006; 86:1009–1031. [PubMed: 16816144]
15. Abbott NJ, Ronnback L, Hansson E. Astrocyte-endothelial interactions at the blood-brain barrier. Nat Rev Neurosci. 2006; 7:41–53. [PubMed: 16371949]
16. Attwell D, Buchan AM, Charpak S, Lauritzen M, Macvicar BA, Newman EA. Glial and neuronal control of brain blood flow. Nature. 2010; 468:232–243. [PubMed: 21068832]
17. Pekny M, Nilsson M. Astrocyte activation and reactive gliosis. Glia. 2005; 50:427–434. [PubMed: 15846805]
18. Sofroniew MV, Vinters HV. Astrocytes: biology and pathology. Acta Neuropathol. 2010; 119:7–35. [PubMed: 20012068]
19. Choi DW, Koh JY, Peters S. Pharmacology of glutamate neurotoxicity in cortical cell culture attenuation by NMDA antagonists. J Neurosci. 1988; 8:185–196. [PubMed: 2892896]
20. Lipton SA. Redox sensitivity of NMDA receptors. Methods Mol Biol. 1999; 128:121–130. [PubMed: 10320978]
21. Szydlowska K, Tymianski M. Calcium, ischemia and excitotoxicity. Cell Calcium. 2010; 47:122–129. [PubMed: 20167368]
22. Danbolt NC. Glutamate uptake. Prog Neurobiol. 2001; 78:560–568.
23. Martinez-Hernandez A, Bell KP, Norenberg MD. Glutamine synthetase: glial localization in brain. Science. 1977; 195:1356–1358. [PubMed: 14400]
24. Albrecht J, Sonnewald U, Waagepetersen HS, Schousboe A. Glutamine in the central nervous system: function and dysfunction. Front Biosci. 2007; 12:332–343. [PubMed: 17127302]
25. Chen Y, Swanson RA. Astrocytes and brain injury. J Cereb Blood Flow Metab. 2003; 23:137–149. [PubMed: 12571445]

NIH-PA Author Manuscript

NIH-PA Author Manuscript

NIH-PA Author Manuscript

26. Mongin AA. Disruption of ionic and cell volume homeostasis in cerebral ischemia: The perfect storm. Pathophysiology. 2007; 14:183–193. [PubMed: 17961999]
27. van Landeghem FK, Weiss T, Oehmichen M, von Deimling A. Decreased expression of glutamate transporters in astrocytes after human traumatic brain injury. J Neurotrauma. 2006; 23:1518–1528. [PubMed: 17020486]
28. Olsen ML, Campbell SC, McFerrin MB, Floyd CL, Sontheimer H. Spinal Cord injury causes a wide-spread, persistent loss of Kir4.1 and glutamate transporter 1: benefit of 17 beta-oestradiol treatment. Brain. 2010; 133:1013–1025. [PubMed: 20375134]
29. Kim Y, Park YK, Cho HY, Kim J, Yoon YW. Long-term changes in expressions of spinal glutamate transporters after spinal cord injury. Brain Res. 2011; 1389:194–199. [PubMed: 21439271]
30. Papadeas ST, Kraig SE, O'Banion C, Lepore AC, Maragakis NJ. Astrocytes carrying the superoxide dismutase 1 (SOD1G93A) mutation induce wild-type motor neuron degeneration in vivo. Proc Natl Acad Sci USA. 2011; 108:17803–17808. [PubMed: 21969586]
31. Rothstein JD, Dykes-Hoberg M, Pardo CA, Bristol LA, Jin L, Kuncl RW, et al. Knockout of glutamate transporters reveals a major role for astroglial transport in excitotoxicity and clearance of glutamate. Neuron. 1996; 16:675–686. [PubMed: 8785064]
32. Yi JH, Hazell AS. Excitotoxic mechanisms and the role of astrocytic glutamate transporters in traumatic brain injury. Neurochem Int. 2006; 48:394–403. [PubMed: 16473439]
33. Baiguera S, Del Gaudio C, Fioravanzo L, Bianco A, Grigioni M, Folin M. In vitro astrocyte and cerebral endothelial cell response to electrospun poly(epsilon-caprolactone) mats of different architecture. J Mater Sci Mater Med. 2010; 21:1353–1362. [PubMed: 19957022]
34. Cao H, Marcy G, Goh EL, Wang F, Wang J, Chew SY. The effects of nanofiber topography on astrocyte behavior and gene silencing efficiency. Macromol. Biosci. 2012; 12:666–674. [PubMed: 22411782]
35. Min SK, Kim SH, Kim CR, Paik SM, Jung SM, Shin HS. Effect of topography of an electrospun nanofiber on modulation of activity of primary rat astrocytes. Neurosci Lett. 2013; 534:80–84. [PubMed: 23178191]
36. Mattotti M, Alvarez Z, Ortega JA, Planell JA, Engel E, Alcantara S. Inducing functional radial glial-like progenitors from cortical astrocytes cultures using micropatterend PMMA. Biomaterials. 2012; 33:1759–1770. [PubMed: 22136716]
37. Biran R, Noble MD, Tresco PA. Directed nerve growth is enhanced by engineered glial substrates. Exp Neurol. 2003; 184:141–152. [PubMed: 14637087]
38. Wang HB, Mullins ME, Cregg JM, McCarthy CW, Gilbert RJ. Varying the diameter of aligned electrospun fibers alters neurite outgrowth and Schwann cell migration. Acta Biomater. 2010; 6:2970–2978. [PubMed: 20167292]
39. Wang HB, Mullins ME, Cregg JM, Hurtado A, Oudega M, Trombley MT, et al. Creation of highly aligned electrospun poly-L-lactic acid fibers for nerve regeneration applications. J Neural Eng. 2009; 6:016001. [PubMed: 19104139]
40. Mongin AA, Hyzinski-Garcia MC, Vincent MY, Keller RW Jr. A simple method for measuring intracellular activities of glutamine synthetase and glutaminase in glial cells. Am J Physiol Cell Physiol. 2011; 301:C814–C822. [PubMed: 21734190]
41. Summers L, Kangwantas K, Nguyen L, Kielty C, Pinteaux E. Adhesion to the extracellular matrix is required for interleukin-1 beta actions leading to reactive phenotype in rat astrocytes. Mol Cell Neurosci. 2010; 44:272–281. [PubMed: 20380881]
42. Ereifej ES, Matthew HW, Newaz G, Mukhopadhyay A, Auner G, Salakhutdinov I, et al. Nanopatterning effects on astrocyte reactivity. J Biomed Mater Res A. 2013; 101:1743–1757. [PubMed: 23184878]
43. Rezakhaniha R, Agianniotis A, Schrauwen JT, Griffa A, Sage D, Bouten CV, et al. Experimental investigation of collagen waviness and orientation in the arterial adventitia using confocal laser scanning microscopy. Biomech Model Mechanobiol. 2012; 11:461–473. [PubMed: 21744269]
44. Arriza JL, Fairman WA, Wadiche JI, Murdoch GH, Kavanaugh MP, Amara SG. Functional comparisons of three glutamate transporter subtypes cloned from human motor cortex. J Neurosci. 1994; 14:5559–5569. [PubMed: 7521911]

NIH-PA Author Manuscript

NIH-PA Author Manuscript

NIH-PA Author Manuscript

45. Rothstein JD, Dykes-Hoberg M, Pardo CA, Bristol LA, Jin L, Kuncl RW, et al. Knockout of glutamate transporters reveals a major role for astroglial transport in excitotoxicity and clearance of glutamate. Neuron. 1996; 16:675–686. [PubMed: 8785064]

46. Koh HS, Yong T, Chan CK, Ramakrishna S. Enhancement of neurite outgrowth using nano-structured scaffolds coupled with laminin. Biomaterials. 2008; 29:3574–3582. [PubMed: 18533251]

47. Xie J, MacEwan MR, Li X, Sakiyama-Elbert SE, Xia Y. Neurite outgrowth on nanofiber scaffolds with different orders, structures, and surface properties. ACS Nano. 2009; 3:1151–1159. [PubMed: 19397333]

48. Schnell E, Klinkhammer K, Balzer S, Brook G, Klee D, Dalton P, et al. Guidance of glial cell migration and axonal growth on electrospun nanofibers of poly-epsilon-caprolactone and a collagen/poly-epsilon-caprolactone blend. Biomaterials. 2007; 28:3012–3025. [PubMed: 17408736]

49. Sheets K, Wunsch S, Ng C, Nain AS. Shape-dependent cell migration and focal adhesion organization on suspended and aligned nanofiber scaffolds. Acta Biomater. 2013; 9:7169–7177. [PubMed: 23567946]

50. Puschmann RB, Zanden C, De Pablo Y, Kirchhoff F, Pekna M, Liu J, et al. Bioactive 3D cell culture system minimizes cellular stress and maintains the in vivo-like morphological complexity of astroglial cells. Glia. 2013; 61:432–440. [PubMed: 23292921]

51. Park E, Velumian AA, Fehlings MG. The role of excitotoxicity in secondary mechanisms of spinal cord injury: a review with an emphasis on the implications for white matter degeneration. J Neurotrauma. 2004; 21:754–774. [PubMed: 15253803]

52. Harvey BK, Airavaara M, Hinzman J, Wires EM, Chiocco MJ, Howard DB, et al. Targeted over-expression of glutamate transporter 1 (GLT-1) reduces ischemic brain injury in a rat model of stroke. PLoS One. 2011; 6:e22135. [PubMed: 21853027]

53. Lee S, Leach MK, Redmond SA, Chong SY, Mellon SH, Tuck SJ, et al. A culture system to study oligodendrocyte myelination processes using engineered nanofibers. Nat Methods. 2012; 9:917–922. [PubMed: 22796663]

NIH-PA Author Manuscript
NIH-PA Author Manuscript
NIH-PA Author Manuscript

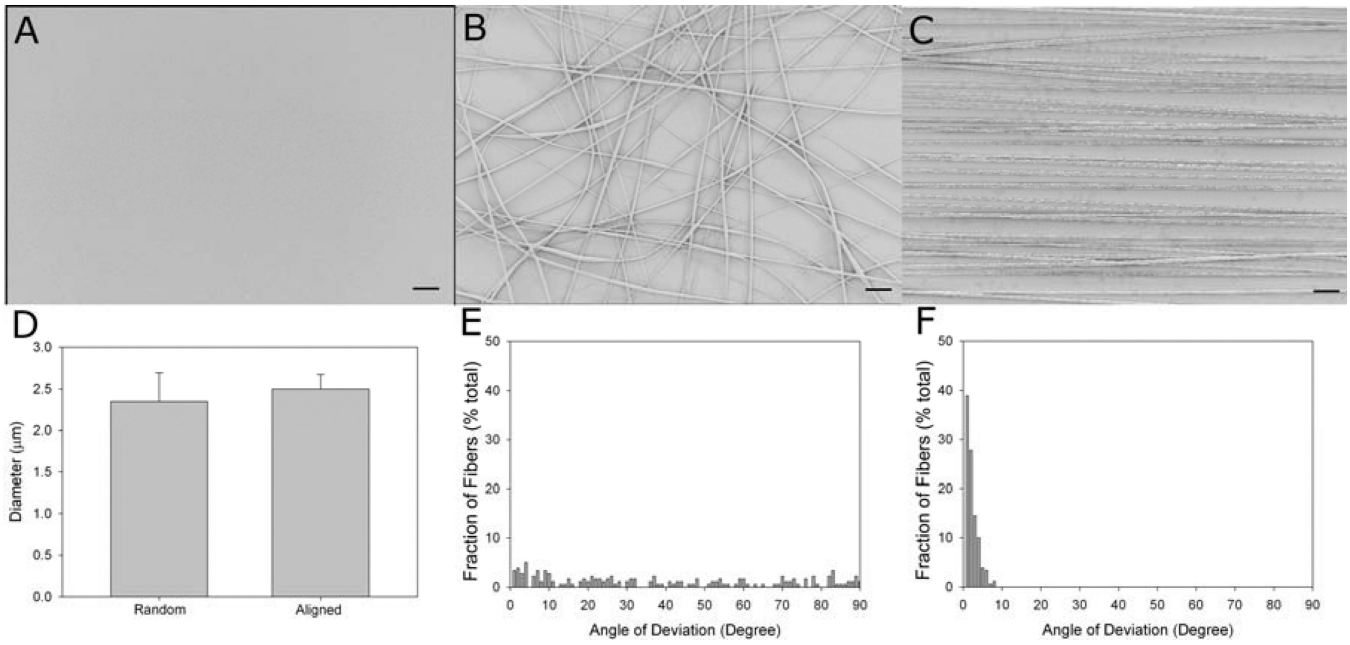

Figure 1.

Characterization of poly-L-lactic acid (PLLA) scaffolds. (a-c) SEM micrographs of PLLA films (a), randomly oriented fibers (b), and aligned fibers (c). (d) Quantitative comparison of fiber diameter for randomly oriented and aligned PLLA fibers. (e-f) Characterization of fiber orientation in randomly oriented (e) and aligned PLLA fiber preparations (f). Scale bars in a-c = 10 μm. Data represented in d and e are the mean values ± SE from three independently fabricated batches.

NIH-PA Author Manuscript
NIH-PA Author Manuscript
NIH-PA Author Manuscript

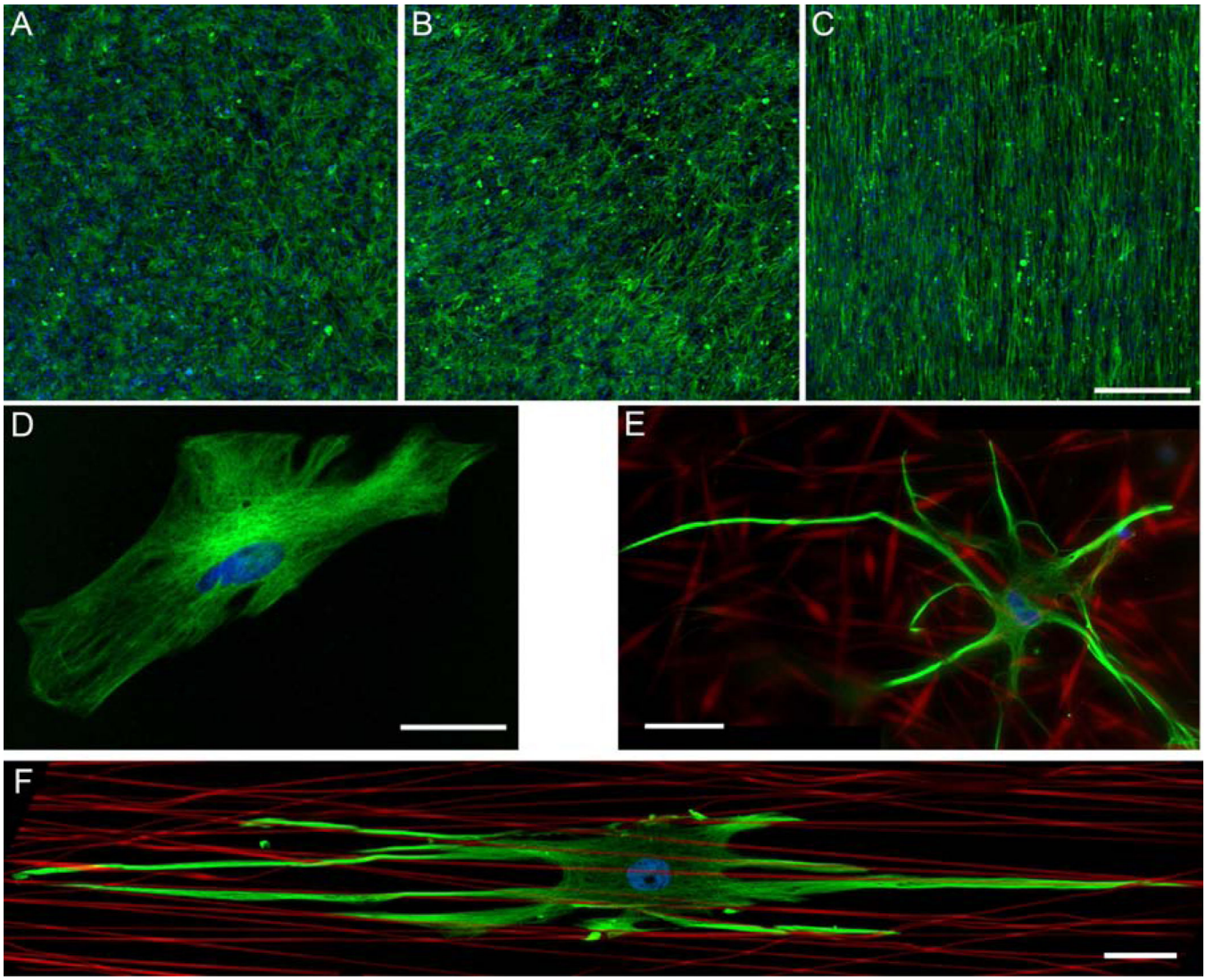

Figure 2.

Fibronectin-coated PLLA scaffolds support strong astrocyte adhesion and proliferation, and PLLA fibers induce formation of astrocytic processes. (a-c) Low magnification (4×) images of astrocytes seeded on PLLA films (a), randomly oriented fibers (b), and aligned fibers (c). Scale bar = 500 μm in c, and the same scale can be applied to images a and b. (d-e) High magnification (40x) images of astrocytes seeded onto PLLA films (d), fluorescently-labeled randomly oriented fibers (e), and fluorescently-labeled aligned fibers (f). Scale bars in d-f = 50 μm. Green signal represents GFAP, blue signal represents the DAPI nuclear stain, and red signal in (e) and (f) is produced by rhodamine contained within the fibers.

NIH-PA Author Manuscript
NIH-PA Author Manuscript
NIH-PA Author Manuscript

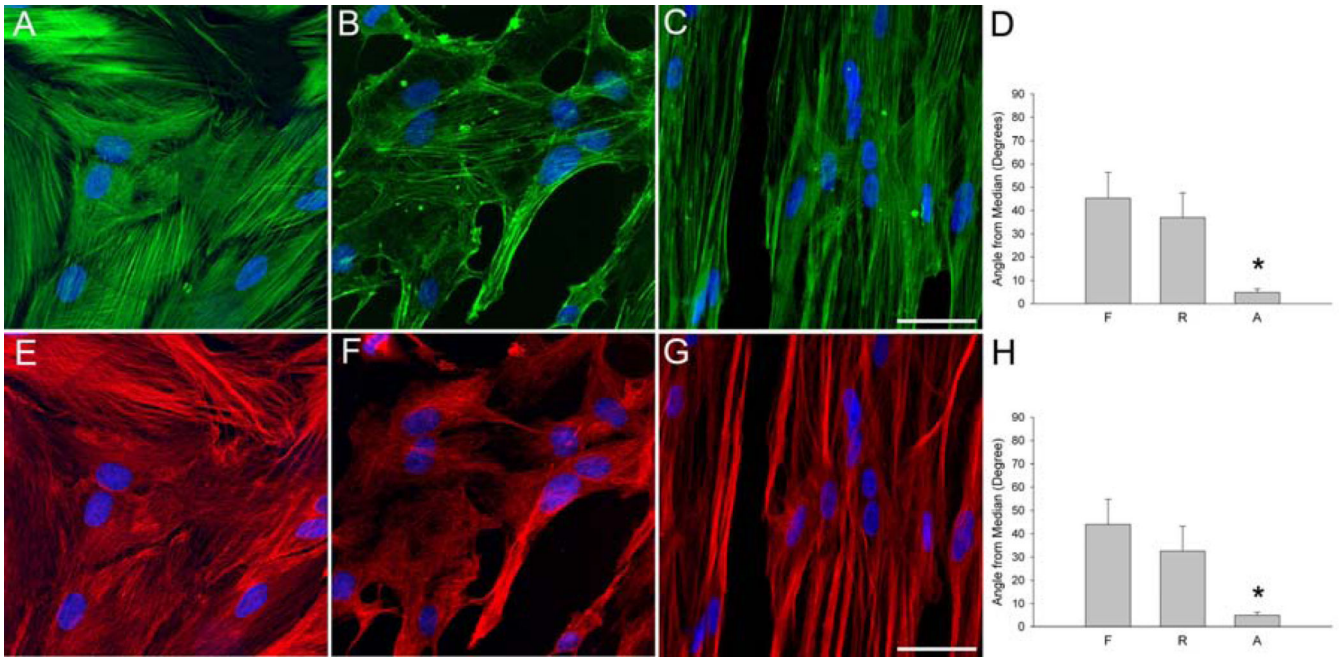

Figure 3.

Aligned PLLA fibers orient actin fibers and microtubules within the astrocyte cytoskeleton. (a-c) Actin staining of astrocytes cultured on fibronectin-coated PLLA films (a), PLLA randomly oriented fibers (b), and PLLA aligned fibers (c). Scale bar = 50 μm in c, and the same scale can be applied to images a and b (d) Quantification of actin alignment. (e-g) Tubulin staining of astrocytes cultured on fibronectin-coated PLLA films (e), PLLA randomly oriented fibers (f), and PLLA aligned fibers (g). Scale bar = 50 μm in g, and the same scale can be applied to images e and f (h) Quantification of tubulin alignment. Data presented in (d) and (h) are the mean values ± SE from three independently prepared cultures. * denotes statistical difference from PLLA films and randomly oriented fibers. F represents film, R represents randomly oriented fibers, and A represents aligned fibers in (d) and (h).

NIH-PA Author Manuscript
NIH-PA Author Manuscript
NIH-PA Author Manuscript

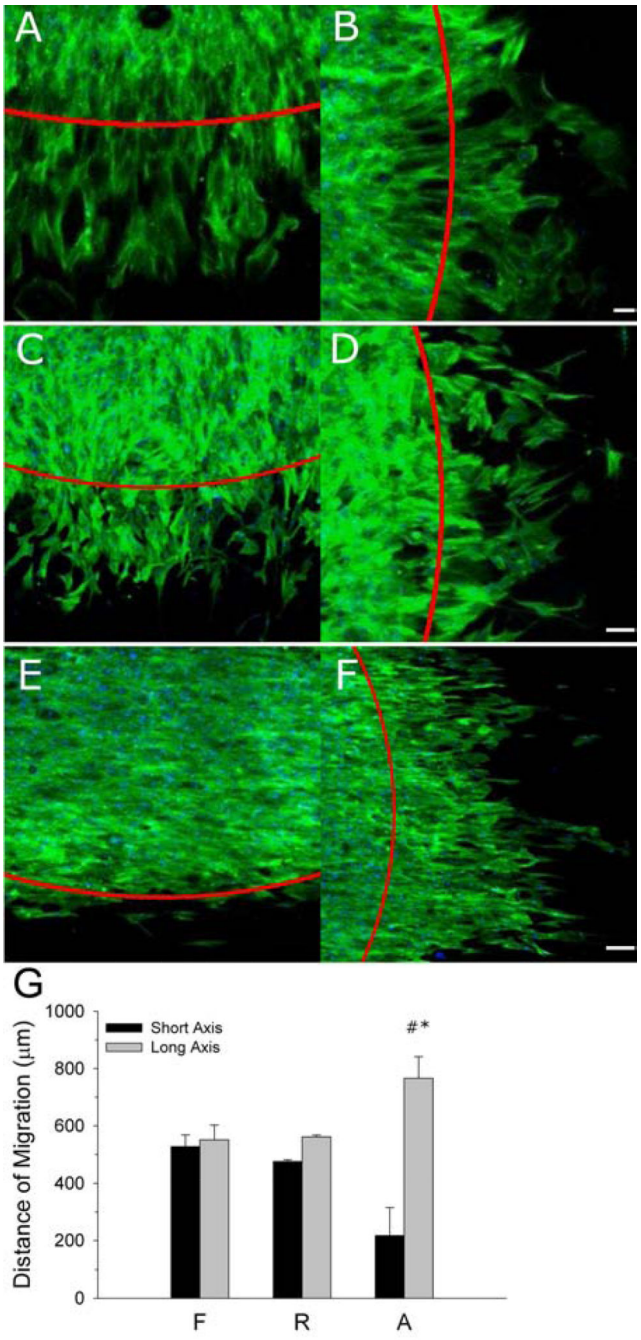

Figure 4.

Aligned PLLA fibers direct and increase the rate of astrocyte migration. (a-f) Phalloidin staining of astrocytes migrating along the “short” and “long” axes for cells plated on fibronectin-coated PLLA films (a-b, scale = 100 μm), randomly oriented PLLA fibers (c-d, scale = 100 μm), and aligned PLLA fibers (e-f, scale = 100 μm). Red arcs indicate initial borders of plated area. (g) Quantification of directed migration along “short” and “long” axes in three experiments. Data presented in g are the mean values ± SE from three independent cultures. *$p<0.05$, “long” vs. “short” axes. $^{\#}$ $p<0.05$, migration distance along

NIH-PA Author Manuscript

NIH-PA Author Manuscript

NIH-PA Author Manuscript

"long" axis on oriented fibers vs. the same parameter for PLLA films and random fibers. F represents film, R represents randomly oriented fibers, and A represents aligned fibers in (g).

NIH-PA Author Manuscript
NIH-PA Author Manuscript
NIH-PA Author Manuscript

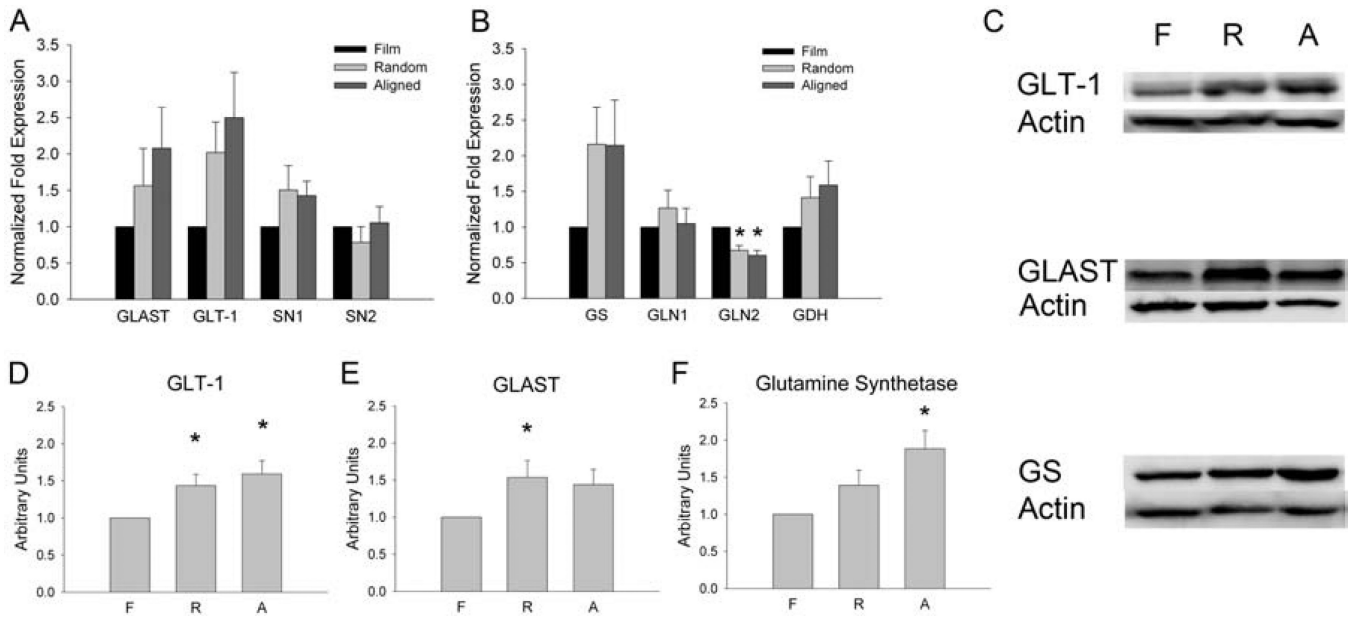

Figure 5.

Plating on PLLA fibers increases expression of the astrocytic transporters, GLT-1 and GLAST, and glutamine synthetase (GS). (a) RT-qPCR analysis of the expression levels for the glutamate transporters GLAST and GLT-1 and the glutamine transporters SNAT3 and SNAT5. Data are the mean values ± SE in six experiments. (b) RT-qPCR analysis of the enzymes of glutamate and glutamine metabolism, including GS, glutaminases 1 and 2 (GLN1, GLN2), and glutamate dehydrogenase (GDH). Data are the mean values ± SE in six experiments. **$p<0.01$, vs. PLLA film. (c) Representative Western blot images of protein expression for glutamate transporters GLT-1 and GLAST, and the metabolic enzyme GS in astrocytes cultured on various substrates. (d-f) Quantitative Western blot analysis of protein expression for GLT-1 (d), GLAST (e), and GS (f). Data are the mean values ± SE from four experiments. *$p<0.05$, vs. PLLA film. F represents film, R represents randomly oriented fibers, and A represents aligned fibers in d, e, and f.

NIH-PA Author Manuscript
NIH-PA Author Manuscript
NIH-PA Author Manuscript

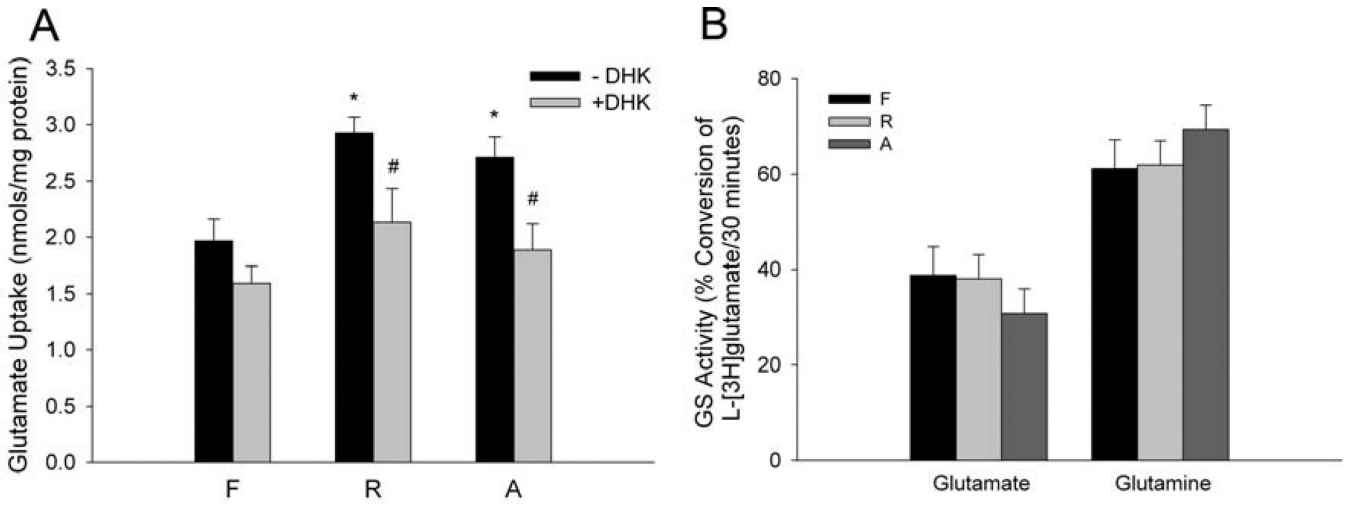

Figure 6.

PLLA fibers increase astrocyte glutamate uptake but do not alter GS activity. (a) $_{l}$-[^{3}H]Glutamate uptake was measured as described in the Methods. The data are the mean values ±SE 10–26 independent assays performed in 3–9 different cultures. 1 mM DHK was used to selectively block GLT-1-mediated glutamate uptake. *$p<0.05$ vs. cell plated on PLLA film. #$p<0.05$ significantly lower vs. cells in the absence of DHK. (b) GS activity, measured as described in the Methods, was not significantly affected by any of the PLLA scaffold topographies. Data are mean values ± SE from six different cultures. F represents film, R represents randomly oriented fibers, and A represents aligned fibers in (a) and (b).

NIH-PA Author Manuscript

NIH-PA Author Manuscript

NIH-PA Author Manuscript

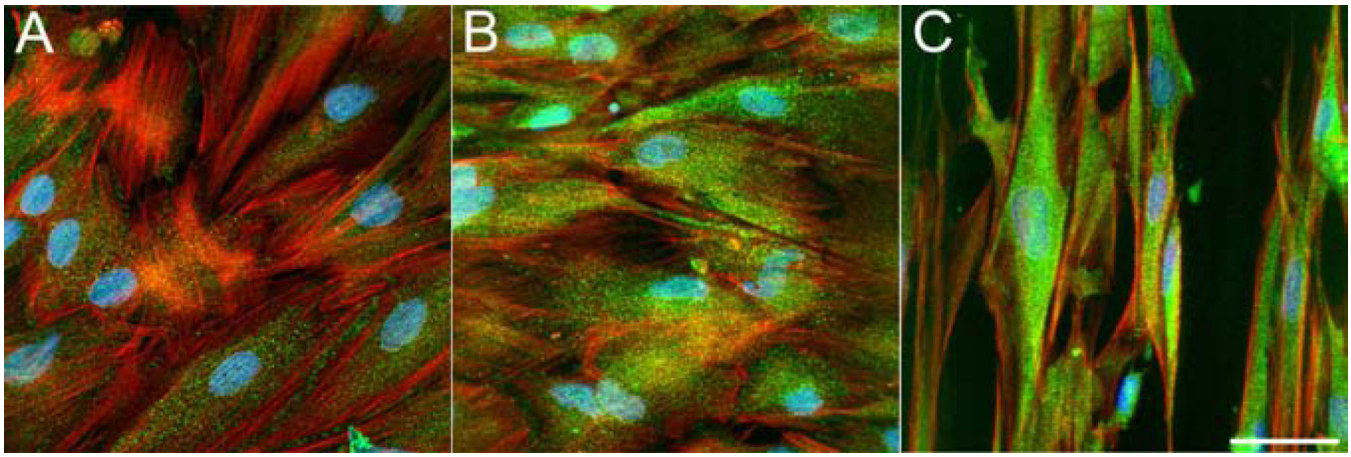

Figure 7.

Immunocytochemical detection of GLT-1 expression. Astrocytes were grown on fibronectin-coated PLLA films (a), randomly oriented PLLA fibers (b), or aligned PLLA fibers (c). Red signal represents actin, green signal represents GLT-1, and blue signal represents DAPI nuclear stain. Scale bar = 50 μm in c, and the same scale can be applied to images a and b.